Universitat Autònoma de Barcelona

Dipòsit digital de documents de la UAB

This is the **accepted version** of the journal article:

Karami-Horestani, Amirhossein; Paredes, Ferran; Martín, Ferran. «High Data Density Absolute Electromagnetic Encoders Based on Hybrid Time». IEEE sensors journal, Vol. 22, Issue 24 (December 2022), p. 23866-23876. DOI 10.1109/JSEN.2022.3216199

This version is available at https://ddd.uab.cat/record/275094

under the terms of the IN COPYRIGHT license

High Data Density Absolute Electromagnetic Encoders Based on Hybrid Time/Frequency Domain Encoding

Amirhossein Karami-Horestani, *Student Member, IEEE*, Ferran Paredes, *Senior Member, IEEE*, and Ferran Martín, *Fellow, IEEE*

***Abstract*—This paper presents a novel concept for the implementation of electromagnetic encoders exhibiting very high data density per unit length (DPL), a figure of merit (FoM) of such systems. Encoding is based on a hybrid scheme that exploits both the frequency and time domains. The encoders consist of rows of inclusions (linear strips) of different sizes, periodically arranged forming a chain (with four columns). The bits corresponding to each row are read sequentially in a time-division multiplexing scheme, whereas the size of the inclusions provides frequency encoding. The main relevant aspect of the proposed system concerns the reader, based on a power splitter architecture with either two outputs (prototype A), or four outputs (prototype B). It is shown that the data capacity per row in one of the encoders read through prototype B is 8.78 bits, whereas the data density is as high as DPL = 29.26 bit/cm, an unprecedented value in this type of encoders. The proposed system can be used as near-field synchronous chipless-RFID system, or as position and velocity sensor. In the latter case, the system is able to provide the absolute encoder position, provided the number of bits per row (or position) is enough to discern the different number of encoder positions (up to 440 different positions for prototype B, corresponding to the indicated number of bits).**

***Index Terms*— Chipless-RFID, electromagnetic encoders, microwave sensors, motion sensors, power splitter.**

I. Introduction

OPTICAL encoders, either linear or rotary, are well-known systems useful for the accurate measurement of positions and velocities in many different scenarios, including elevators, servomechanisms, conveyors, and pointing mechanisms, among others [1]-[3]. The working principle of such encoders is based on the transparency of a set of apertures arranged circularly or linearly on an opaque material (disc in rotary encoders) made of metal, plastic, or glass. When one of such apertures lies in the optical path between the optical source and the photodetector, e.g., a photodiode, a pulse in the form of an electrical signal is generated in the detector, and this provides information relative to the encoder position and velocity. The main advantage of optical encoders is the achievable resolution, determined by the number of pulses per revolution (PPR) in rotary encoders, or by the number of pulses per unit length in the linear counterparts. It should be mentioned that optical rotary encoders exhibiting thousands of pulses per revolution are commercially available. Moreover, optical encoders can be either incremental or absolute. In the latter case, a unique identification (ID) code determines (or is assigned to) the different encoder positions. By contrast, in incremental encoders, the position is given by the cumulative number of pulses recorded from a reference position. Thus, after a system reset, it is necessary to return to that reference position. One of the main drawbacks of optical encoders concerns their limited robustness against harsh environments, such as those subjected to pollution, dirtiness, or grease, encountered in many industrial systems.

The solution to the previous limitative aspect of optical encoders is the use of magnetic fields or microwaves, more tolerant to the effects of pollution and dirtiness. Magnetic and inductive encoders, as well as Hall-effect sensors, constitute an interesting alternative to optical encoders [4]-[12], but such systems are based on magnets or inductive coils, and are not absent of certain complexity. Recently, a new type of encoder systems, based on the effects that a chain (or chains) of inclusions etched or printed on a dielectric slab (a disc in rotary

This work was supported by MCIN/AEI 10.13039/501100011033, Spain, through the projects PID2019-103904RB-I00 (ERDF European Union) and PDC2021-121085-I00 (European Union Next Generation EU/PRTR), by the AGAUR Research Agency, Catalonia Government, through the project 2017SGR-1159, and by Institució Catalana de Recerca i Estudis Avançats (who awarded Ferran Martín). A. Karami-Horestani acknowledges MCIN/AEI /10.13039/501100011033 and ESF for Grant PRE2020-093239.

A. Karami-Horestani, F. Paredes, and F. Martín are with GEMMA/CIMITEC, Departament d'Enginyeria Electrònica, Universitat Autònoma de Barcelona, 08193 Bellaterra, Spain. (e-mail: Ferran.Martin@uab.es).

XXXX-XXXX © XXXX IEEE. Personal use is permitted, but republication/redistribution requires IEEE permission.
See http://www.ieee.org/publications_standards/publications/rights/index.html for more information.

encoders) generate on a transmission line feed by a single harmonic signal (or by a set of harmonic signals), has been proposed [13]. Such encoders have been designated as electromagnetic (or microwave) encoders, and both rotary [13]-[17] and linear [18]-[28] implementations have been reported.

The working principle of electromagnetic encoders has been reported in the previous works and also in the monographs [29], [30]. In brief, a chain, or various chains, of (typically, although not exclusively) metallic inclusions printed or etched in the movable element, made of a dielectric material, modulate the transmission coefficient of a transmission line based structure. There are specific frequencies where the excursion experienced by the transmission coefficient by encoder motion is significant. Thus, encoder motion modulates the amplitude of the output signal at those carrier) frequencies, and the envelope functions contain as many peaks, or dips, as inclusions in the corresponding chain/s. Thus, from such envelope functions, it is possible to retrieve the information relative to the encoder velocity, position and motion direction.

In electromagnetic rotary encoders, a PPR of 1200 has been demonstrated [16]. The device reported in [16] is able to detect the motion direction, clockwise and counter-clockwise (the rotary encoders reported in [14]-[18] are incremental). Linear electromagnetic encoders based on different types of inclusions, including linear strips [18], [19] and metallic patches [23], [25], [27], have been reported. It is also remarkable that electromagnetic encoders based on dielectric inclusions have been proposed. Such encoders are based on permittivity contrast [20]-[22]. In incremental-type electromagnetic encoders, typically a single chain of inclusions suffices (unless detection of the motion direction is necessary [16]). Such chain contains all the inclusions at the predefined positions in the chain. Thus, such periodic chain provides a periodic envelope function, and the encoder velocity is determined from the time lapse between adjacent peaks (or dips), whereas the position is retrieved from the cumulative number of pulses from a reference position.

To the best of the authors' knowledge, absolute electromagnetic encoders have not been reported to date. Nevertheless, an approximation to absolute encoders was first reported in [23], and then improved in various works [25], [27]. In such encoders, designated as quasi-absolute (but not absolute), one chain is equipped with a certain ID code, and is used to determine the encoder position, whereas another chain, periodic, is used as a clock for synchronization purposes, and provides the encoder velocity. However, concerning the position chain, a single bit, i.e., presence or absence of a functional inclusion, is attributed to each position, which is not useful to discern the encoder location. Thus, the strategy, first proposed in [23], to solve this limitation was to consider a certain subset of N consecutive inclusions satisfying

$$N \geq \log_2\left(\frac{L}{p}\right) \tag{1}$$

where L is the encoder length and p is the encoder period (or spatial resolution), so that L/p is the number of different encoder positions. If the whole encoder chain is codified according to the so-called De Bruijn sequence [31], the ID sub-code corresponding to any subset of N consecutive inclusions does not repeat. Thus, the position can be determined by reading the bit corresponding to that position, plus the previous $N-1$ bits. However, after a system reset, the encoder should displace N positions for retrieving its specific location. For this main reason, this type of encoders cannot be categorized as absolute. Let us mention that the instants of time for reading the bits of the position chain are determined by the clock signal, generated by the (periodic) clock (or velocity) chain, with all inclusions present at their specific locations.

In this work, it is demonstrated that the number of bits per encoder position can be significantly enhanced by considering inclusions (linear strips in this paper) of different length. This provides frequency encoding, and, consequently, the system combines both the frequency and the time domain, as far as the ID codes for the different encoder positions, are inferred sequentially, in a time division multiplexing scheme. The idea of frequency encoding in electromagnetic encoders was proposed in [32] by using C-shaped resonators, and in [33], [34] by using linear strips of different dimensions. In this work, the data capacity per encoder position is enhanced by considering four columns of inclusions, and by designing a specific reader topology, based on a power splitting scheme. A very preliminary idea was reported in [35] by using two columns of inclusions and a two-output power splitter reader, resulting in 4.58 bits per position (or row). In the present paper, it is demonstrated that by using four inclusions' columns and a reader based on a four-output power splitter (prototype B), the number of bits per position increases to 8.78 bits. Taking into account the inclusions' chains period, the resulting data density per unit length in one of the encoders is as high as DPL = 29.26 bit/cm, an unprecedented value in this type of encoders.

The paper is organized as follows. The proposed absolute electromagnetic encoder concept and the working principle are reported in Section II. In section III, the specific designed systems, designated as A and B, are presented. In encoder type A, the movable part consists of four columns of inclusions (linear strips of different size), whereas the reader is based on a two-output power splitter. In encoder type B, the difference is that the reader is a four-output power splitter (this notably increases the inclusions' combinations, as it will be shown, and, consequently, the number of bits per encoder position). Experimental validation of the proposed concept is demonstrated in Section IV. A comparative analysis with other electromagnetic encoders is given in Section V. Finally, section VI concludes the work.

II. Absolute Electromagnetic Encoder Concept and Working Principle

The absolute electromagnetic encoders of this paper, consisting of four columns, or chains, of linear strips (of four different sizes), oriented transversally to the axis of the chains, and etched on a dielectric substrate, are inspired by the encoders proposed in [35], based on two chains. The increase in the

number of bits per position in such two-chain encoders, as compared to those based on a single chain [32]-[34], is clear. Namely, one of the chains provides 5 different states per position, corresponding to the four different strip lengths, plus an additional state associated to the absence of strip (this latter possibility was not considered in [35]). The same applies to the second chain. Consequently, this gives 5 × 5 = 25 different states per encoder position. However, the simultaneous absence of inclusion in both chains for a given position should be avoided, since at least one strip is required for the (necessary) synchronism of the encoder. Thus, the total number of states is 25 – 1 = 24, corresponding to 4.58 bits per position. For the detection of the specific state (or ID code) associated to each position (encoder reading), a reader based on a power splitter configuration, arranged in T-shape, was proposed in [35]. See in Fig. 1 the perspective view of the system, and the photograph of the reader and a specific encoder reported in [35]. By displacing the encoder over the reader, the input signal is prevented to be transmitted to the output port (either 2 or 3) when a strip lies on top of the corresponding output port access line, provided the frequency of such signal is tuned to the value associated to such specific strip (which depends on its length). Namely, when a strip is on top of a line, a notch in the frequency response, controlled by the strip length, is generated. This means that for tag reading, as many harmonic signals as strip sizes (i.e., four) are needed, and such signals should be injected to the input port of the splitter. For that purpose, a combiner provides a solution, as it was adopted in [16]. Alternatively, a microcontroller can be used in order to inject the harmonic feeding signals at different instants of time, the approach used in [27].

The detection of each specific strip is revealed by the reduction in the amplitude of the corresponding injected (carrier) signal at the corresponding output port (port 2 for the left chain, and port 3 for the right chain). In other words, each injected carrier signal is amplitude modulated (AM) by encoder motion, i.e., by strip overlapping with the access lines of the output ports, and the envelope functions contain the ID code. Obviously, the absence of strip in any of the chains (but not in both chains simultaneously, as justified due to synchronization) does not reduce the amplitude of the feeding signals at the corresponding port, and therefore can also be detected. Note that for retrieving the ID code for each encoder position (or row), the envelope functions of each carrier signal should be inferred at both output ports of the splitter (the architecture of this system is depicted in Fig. 2).

According to the previously explained scheme, or working principle, encoder reading proceeds sequentially, row by row, as the encoder is displaced over the reader. However, the states (or ID codes) corresponding to each row are generated by frequency encoding (through the length of the strips). For this reason, it is considered that the proposed encoder system exploits both the frequency and the time domains simultaneously (hybrid approach).

In order to enhance the data capacity per row, one possibility is to add further chains to the encoder. Particularly, encoders with four chains of linear strips, and also with four possible lengths (and hence requiring four carrier signals for encoder reading), are proposed in this work. This represents a significant

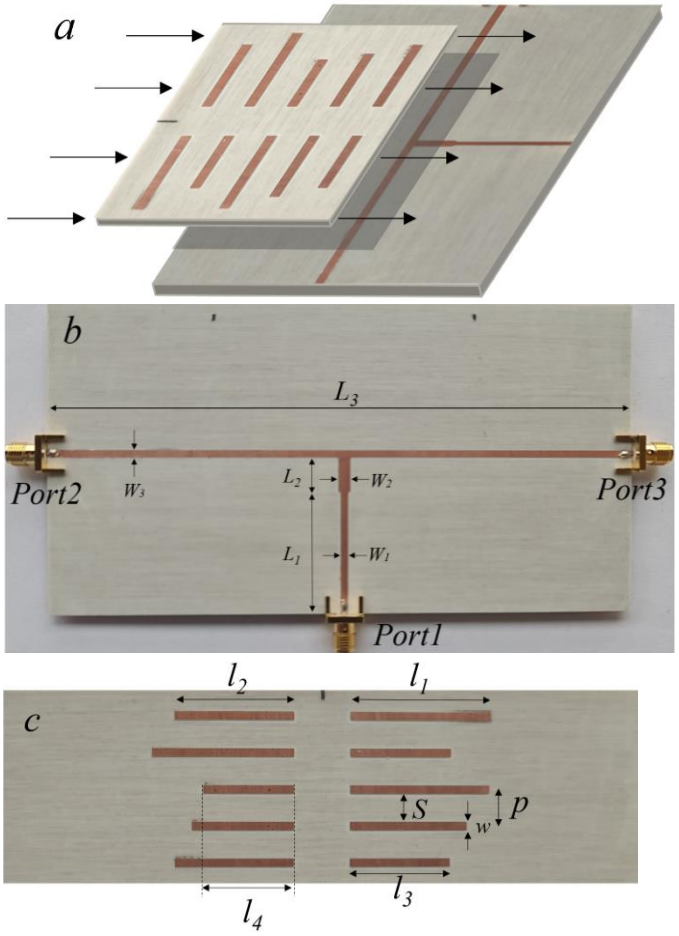

Fig. 1. Perspective view of the proposed encoder system (a), and photograph of the power splitter microstrip reader (b) and a specific encoder with two chains of inclusions (c). Relevant dimensions are indicated (note that l_i with i = 1, 2, 3, 4 indicates the strip length). The encoder is uncoated in the back substrate side, whereas the reader has a ground plane metallization in the back substrate size.

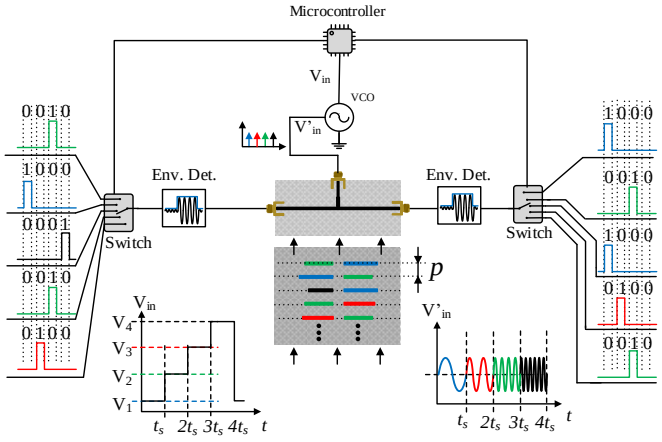

Fig. 2. Sketch showing the working principle of the hybrid time/frequency domain near-field chipless-RFID system based on a two-chain encoder and power splitter reader with two output ports. The VCO generates four harmonic signals, managed by a microcontroller, in order to detect the different sizes of the chain inclusions (frequency encoding is achieved through the size of the inclusions, as indicated in the text).

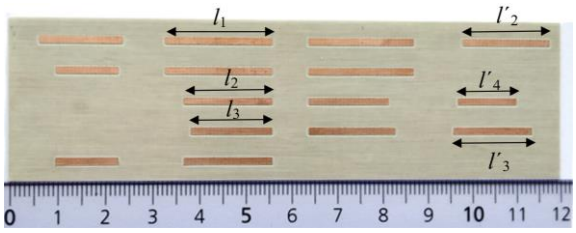

Fig. 3. Photograph of a specific encoder with four chains of inclusions.

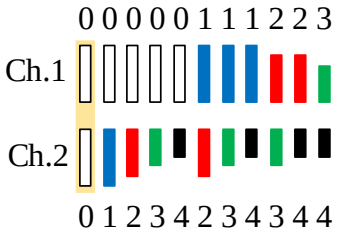

Fig. 4. Possible combinations (11) of strips for the two pairs of chains of the encoder. Absence of strip is labeled as '0' and the other four labels correspond to the different strip lengths.

enhancement in the data capacity of the encoder, as it will be demonstrated in the next section. Nevertheless, it will also be shown in that section that by using a reader based on a power splitter with four output ports, conveniently designed, the data capacity can be further increased (this constitutes the main relevant contribution of the present paper).

III. Specific Encoder Systems Design

The first encoder system proposed in this paper, designated as encoder type A is based on a two-output power splitter reader and four-chain encoders. The second system uses a four-output splitter reader and four-chain encoders (encoder type B). Let us next discuss in detail both systems separately.

A. Encoder type A: two-output splitter reader and four-chain encoder

For encoder type A, the considered reader is the one depicted in Fig. 1(a), whereas the encoder consists of four chains of linear strips (with four possible different lengths, as indicated). Reader dimensions, in reference to Fig. 1(a), are $L_1 = 31.20$ mm, $L_2 = 8.80$ mm, $L_3 = 150.00$ mm, $W_1 = 1.80$ mm, $W_2 = 2.98$ mm, and $W_3 = 1.80$ mm. The reader was implemented on the *Rogers 4003C* substrate with dielectric constant $\varepsilon_r = 3.55$, thickness $h = 0.81$ mm and loss factor $\tan\delta = 0.0022$. The photograph of a specific encoder, implemented on an identical substrate to that of the reader, is depicted in Fig. 3. Dimensions are: $l_1 = 23.0$ mm, $l_2 = 19.0$ mm, $l_3 = 16.5$ mm, $l_4 = 12$mm, $l'_1 = 23.5$mm, $l'_2 = 19.5$ mm, $l'_3 = 17.0$ mm, and $l'_4 = 12.5$ mm. The super-index (') corresponds to the dimensions in the outer columns, slightly enhanced to preserve the same resonance frequency. When the encoder is in relative motion to the reader, two chains should lie to the left and two chains should lie to the right of the imaginary line given by the axis of the input access line (this determines the minimum length of the output access lines). By this means, the possible states per row are significantly higher than the 24 states of the encoder system reported in [32]-[34], and briefly discussed in the previous section. Let us next analyze this aspect.

Obviously, not all the possible combinations of two strips at both sides of the axis of the input line can be detected. Particularly, the presence of two identical strips in one of the sides of a row, e.g. in the right hand side chain, cannot be discerned from the case of only one of such strips present (and the other absent), as far as they provide a notch at the same carrier frequency. Nevertheless, the absence of strips in both chains, either situated to the left or to the right of the input line axis, can be perfectly detected by the absence of a dip in any of the envelope functions. On the other hand, the placement of two different strips provides the same result in the corresponding output port, regardless of the specific position. Thus, the number of possible states for each pair of chains is given by the so-called combinations of $m = 5$ elements (absence of strip plus four different strips) taken in groups of $n = 2$ elements (two chains), where repetition is not possible and the order does not matter. The expression is as follows.

$$C_m^n = \frac{m!}{n!\,(m-2)!} = 10 \qquad (2)$$

This gives 10 possible combinations. However, exceptionally, absence-absence of strips can be detected, as mentioned, and therefore the number of possible states for each pair of chains is 11 (see those combinations in Fig. 4). This gives a total of 11 x 11 = 121 possible states, but the state corresponding the absence of the four strips should be avoided for synchronization reasons, as explained before. Therefore, the total number of states per row (or position chain) is 121 – 1 = 120, corresponding to 6.9 bits.

B. Encoder type B: four-output splitter reader and four-chain encoder

The main limitation of the system described in Section III.A is the impossibility to distinguish states (for either of the two chains at both sides of the main axis of the splitter) where the order of the strips is interchanged [e.g., (1,2) and (2,1), according to the nomenclature of Fig. 3]. To solve this aspect, a reader based on four, rather than two, outputs, conveniently disposed, is proposed. The layout of such splitter is depicted in Fig. 5. The dimensions of the reader, implemented on the *Rogers 4003C* substrate with dielectric constant $\varepsilon_r = 3.55$, thickness $h = 0.81$ mm and loss factor $\tan\delta = 0.0022$, are given in the caption of Fig. 5, whereas the encoder dimensions are: $l_1 = 26.2$mm, $l_2 = 24$mm, $l_3 = 20.5$mm, $l_4 = 17.5$mm, $l'_1 = 27.5$mm, $l'_2 = 25$mm, $l'_3 = 22$mm, $l'_4 = 18.5$mm [see Fig. 10(a)].

In view of the splitter topology and encoder displacement over the reader (with two chains at both sides of access line of port 4 and two chains at both sides of access line of port 2), it

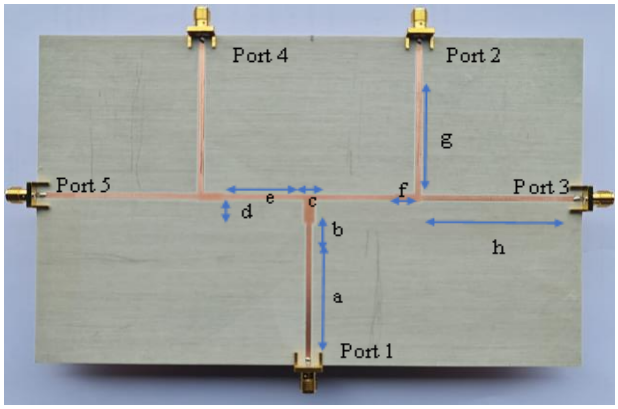

Fig. 5. Photograph of the four-output power splitter reader. Dimensions of the reader (in mm) are: a = 51.5, b = 8.5, c = 4, d = 3, e = 27.5, f = 7, g = 58, h = 56. Dimensions of the access lines, as well as the distance between the different T-junctions, has been determined to accommodate displacement of the chains over the reader as indicated in the text, namely, with two chains at both sides of access line of port 4 and two chains at both sides of access line of port 2.

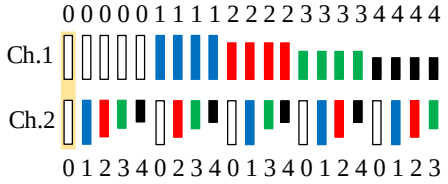

Fig. 6. Possible combinations (21) of strips for the two pairs of chains of the encoder. Absence of strip is labeled as '0' and the other four labels correspond to the different strip lengths.

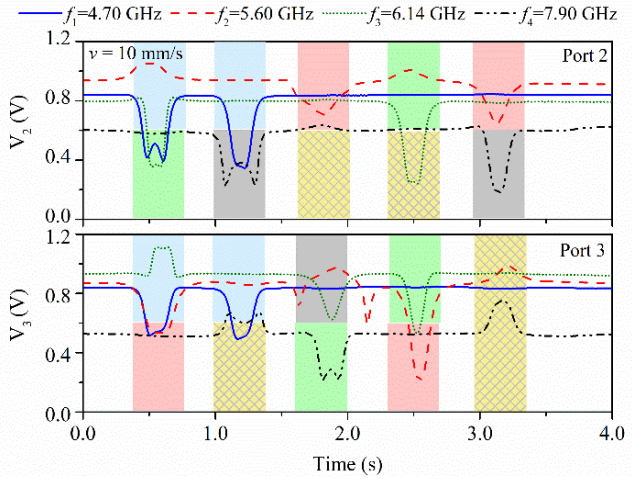

Fig. 7. Envelope functions of the four-column and five-row encoder of Fig. 3, recorded at ports 2 and 3 with the reader of Fig. 1(a), prototype A.

follows that with the configuration of Fig. 5, the order of the strips among the pair of chains can be distinguished (however, repetition of elements should be avoided). For example, the state (1,0) and (0,1) can be distinguished, but (1,1) provides the same result than (1,0). Thus, the number of possible different states is given in this case by the so-called variations of n = 2 elements taken among m = 5 elements, given by:

$$V_m^n = \frac{m!}{(m-n)!} = 20 \qquad (3)$$

Note, however, that, similar to the previous case, the state (0,0) should be exceptionally considered, and thus the number of possible states is 21 × 21 = 441, minus the state where all the strips of the four chains are absent. The 21 possible combinations for the two pairs of chains are depicted in Fig. 6. This gives a total number of 440 different states, corresponding to 8.78 bits per row, a competitive number.

IV. Experimental Validation

Both systems, encoder type A and encode type B, have been experimentally validated by considering three specific encoders with different ID.

A. Results for encoder type A

Figures 7, 8, and 9 depict the three considered four-chain encoders for experimental validation of the system designated as A, based on the reader of Fig. 1(a). Note that, for each figure (or specific encoder), two graphs are depicted, corresponding to the envelope functions of the four signals recorded at both output ports of the reader. The specific (carrier) frequencies of the four signals are f_1 = 4.70 GHz, f_2 = 5.60 GHz, f_3 = 6.14 GHz, f_4 = 7.90 GHz, where the sub-index is the same used for the identification of the length of the strips. For better understanding of the results of Figs. 7, 8, and 9, different colors are assigned to each signal frequency. According to these figures, a perfect correlation between the strips present at each row and the dips of the envelope functions is found. Nevertheless, let us mention that in the validation of this proposed proof-of-concept, rather than using either a combiner or a microcontroller for injecting the four harmonic signals, such signals have been injected separately. Retrieving the envelope functions has been carried out by means of an envelope detector, which has been implemented by means of a Schottky diode (model *Avago HSMS- 2860*) and the *N2795A* active probe (with capacitance C = 1 pF and resistance R = 1 MΩ). The input signals have been injected by means of the network analyzer *Agilent N5221A*. Finally, the envelope functions have been recorded by means of an oscilloscope, model *Agilent MSO-X 3104A*. Let us also mention that for the mechanical displacement of the encoder over the reader the linear displacement system model *Thorlabs LTS300/M has* been used. The displacement velocity of the encoders was set to v = 10 mm/s, but a constant velocity is not necessary. The photograph of the experimental setup in depicted in Fig. 10.

Taking into account the period of the encoders of Figs. 7, 8, and 9 (p = 1.0 cm), and the number of bits per row (6.9) bits, the resulting density of bits per unit length is DPL = 6.9 bit/cm. Concerning the density per surface, it is found to be DPS = 0.575 bit/cm^2 (note that the width of these four-chain encoders is 12 cm). Nevertheless, the relevant figure of merit in these encoders is the DPL, rather than the DPS, since the main goal is to accommodate as much number of bits per row as possible.

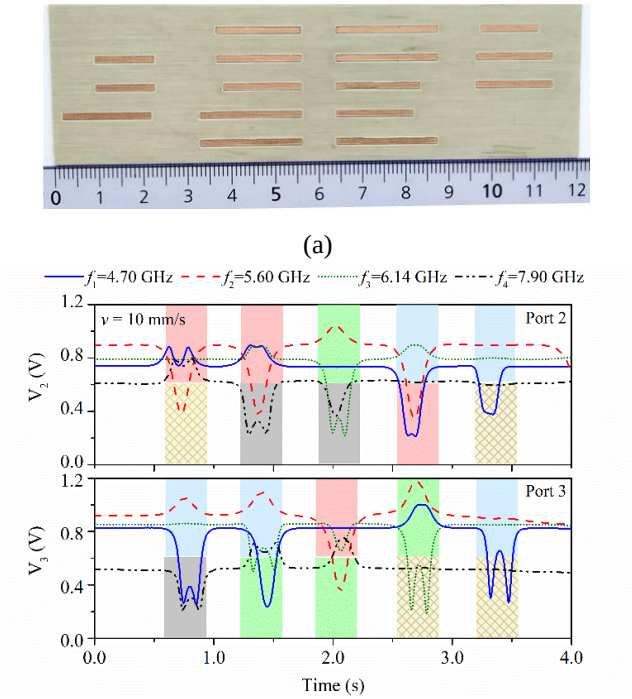

Fig. 8. Four-column and five-row encoder (a) and the corresponding envelope functions recorded at ports 2 and 3 (b) with the reader of Fig. 1(a), prototype A.

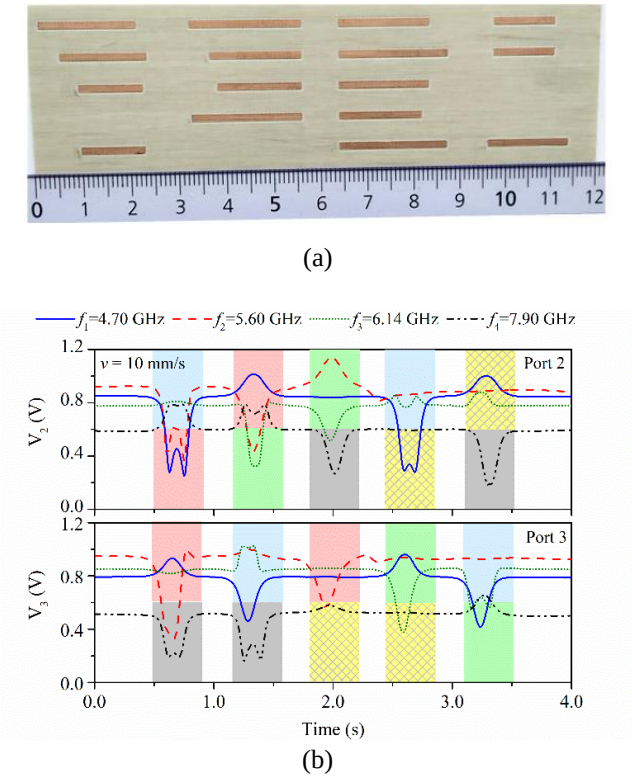

Fig. 9. Four-column and five-row encoder (a) and the corresponding envelope functions recorded at ports 2 and 3 (b) with the reader of Fig. 1(a), prototype A.

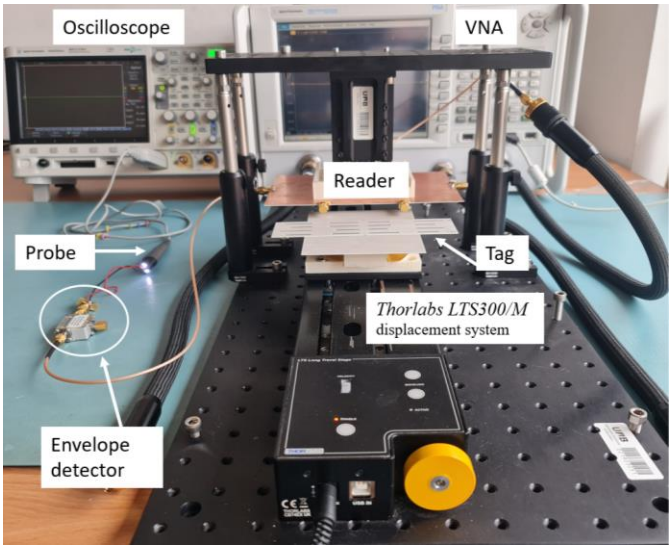

Fig. 10. Photograph of the experimental setup.

B. *Results for encoder type B*

Figures 11, 12, and 13 depict the three considered four-chain encoders for experimental validation of the system designated as B, based on the reader of Fig. 5. In this case, for each specific encoder, four graphs are depicted, corresponding to the envelope functions of the four signals recorded at the four output ports of the reader. The specific (carrier) frequencies of the four signals are in this case f_1 = 4.22 GHz, f_2 = 4.55 GHz, f_3 = 5.24 GHz, f_4 = 6.01 GHz (see Fig. 11), but for Figs. 12 and 13 such frequencies have been slightly tuned, as indicated in the figures. According to Figs 11, 12, and 13, a perfect correlation between the strips present at each row and the dips of the envelope functions is found. The density of bits in this case is DPL = 8.78 bit/cm and DPS = 1.90 bit/ cm^2, significantly improved as compared to system A, due the enhanced number of bits per encoder row.

We should mention that in the design of the four-chain encoders presented so far, we have been a bit conservative, in order to clearly distinguish the dips in the envelope functions. Thus, with the objective of improving the DPL as much as possible, we have fabricated additional four-chain encoders with smaller periods, i.e., one encoder with a period of p = 0.5 cm and another one with the period set to p = 0.3 cm. The optimum period has been found to be p = 0.3 cm. For smaller periods, the encoders cannot be correctly read. Figure 14 shows a four-chain encoder with p = 0.5 cm and the corresponding envelope functions, which again, perfectly correlate with the ID code of the encoder (let us designate this system, with encoders with smaller period, as B', in order to differentiate it from the previous one, designated as B). Figure 15 shows the encoder with the period of p = 0.3 cm, as well as the results for that encoder system (prototype B''). The figure of merit in these cases are DPL = 17.56 bit/cm for the encoder with the period of p = 0.5 cm, and 29.26 bit/cm for the encoder with the period of p = 0.3 cm, unprecedented values in this type of electromagnetic encoders, to the best of authors' knowledge.

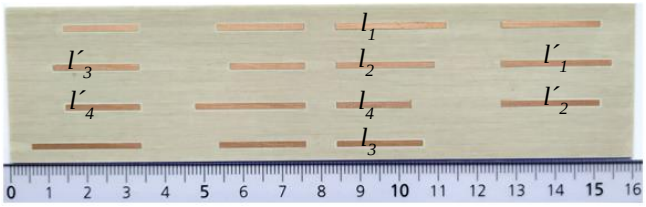

(a)

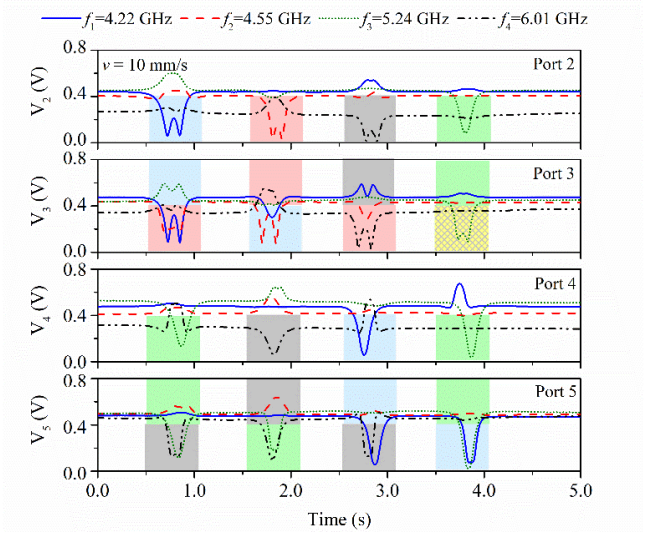

(b)

Fig. 11. Four-column and four-row encoder (a) and the corresponding envelope functions recorded at ports 2, 3, 4 and 5 (b) with the reader of Fig. 5, prototype B.

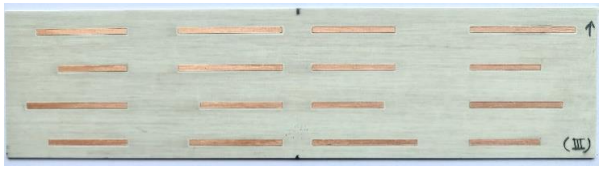

(a)

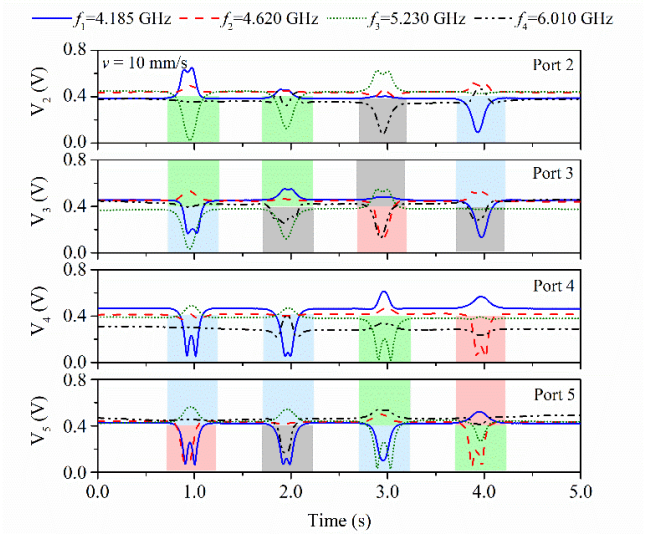

(b)

Fig. 12. Four-column and four-row encoder (a) and the corresponding envelope functions recorded at ports 2, 3, 4 and 5 (b) with the reader of Fig. 5, prototype B.

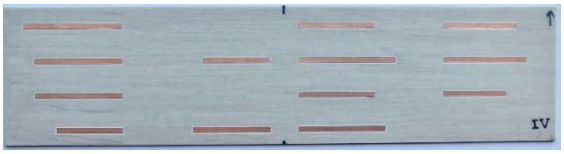

(a)

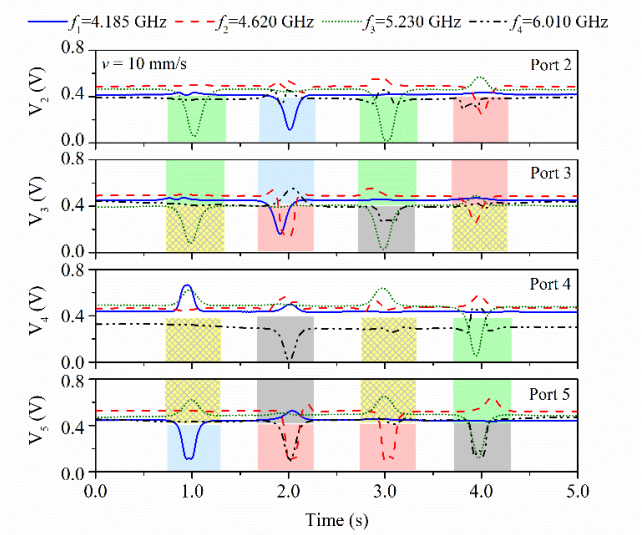

(b)

Fig. 13. Four-column and four-row encoder (a) and the corresponding envelope functions recorded at ports 2, 3, 4 and 5 (b) with the reader of Fig. 5, prototype B.

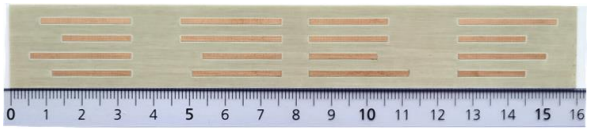

(a)

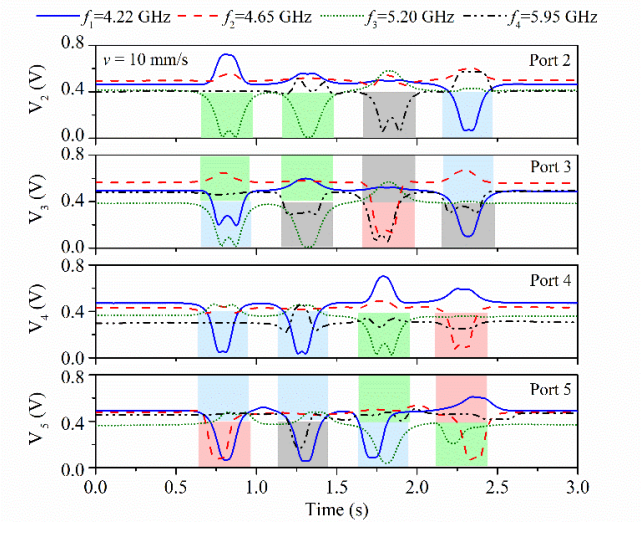

(b)

Fig. 14. Four-column and four-row encoder with improved period p = 0.5 cm (a) and the corresponding envelope functions recorded at ports 2, 3, 4 and 5 (b) with the reader of Fig. 5, prototype B'.

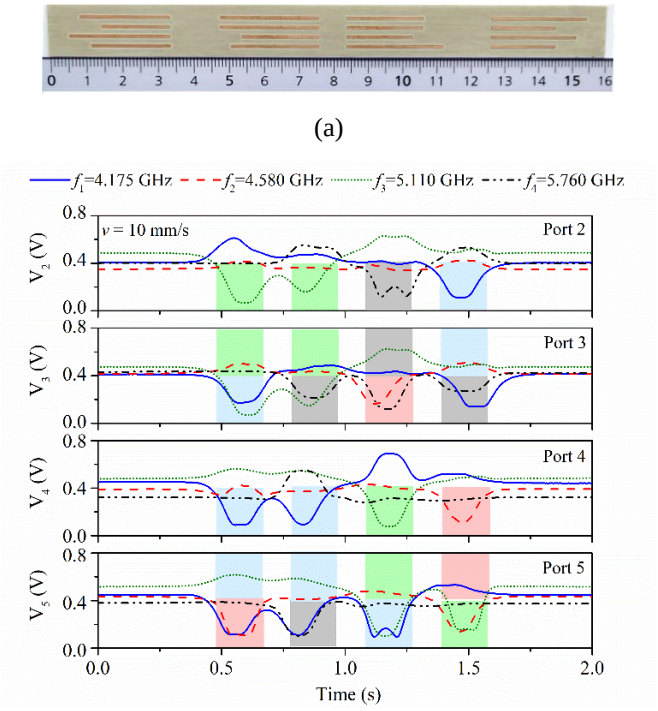

Fig. 15. Four-column and four-row encoder with optimized period p = 0.3 cm (a) and the corresponding envelope functions recorded at ports 2, 3, 4 and 5 (b) with the reader of Fig. 5, prototype B''.

Let us comment that lateral (transverse) potential misalignments between the reader and the encoder can be tolerated with the present system, as far as the reader dimensions have been conservatively calculated so that when the encoder moves over the reader, the strip inclusions of the chains do not lie on top of access lines of ports 1 for sensor type A, and ports 1, 2 and 4 for sensor type B, B' and B''.

V. Comparative Analysis and Discussion

A. Functionality as motion sensor

The main advantageous aspect of the electromagnetic encoders proposed in this paper is the number of bits per encoder row (or position), as high as 8.78 bits in the system identified as B, with four-chain encoders and four output port splitter reader. By contrast, system A, with four-chain encoders and two output port splitter reader, exhibits 6.9 bits per row. Systems A and B represent an improvement as compared to the system presented in [35], based on a two output port power splitter reader, but considering encoders with only two chains (with 4.58 bits per row). In the electromagnetic encoder systems reported in [32]-[34], frequency was also used for encoding, but with a single encoder chain and four different inclusion dimensions, only 2 bits per row where achieved. Nevertheless, this represented an improvement as compared to the former systems, without frequency encoding, and based merely on the presence or absence of functional inclusions at the predefined positions of the (single) chain [18], [19], [23], [24], [26], [27], [36]-[39]. An additional chain in some of these systems was used for synchronization purposes [23], [24], [26], [27], [36]-[38].

Concerning the data density, there are two relevant figures of merit (FoM), i.e., the density per length (DPL) and the density per surface (DPS). However, in electromagnetic encoders, the main goal is to accommodate as much bits as possible in the minimum possible length. Thus, the key FoM is the DPL, as high as DPL = 17.56 bit/cm in the prototype designated as B' in the previous section (with encoder period of p = 0.5cm) and even higher in the prototype B'' (DPL = 29.26 bit/cm), with p = 0.3 cm. Note that these values of the DPL are superior to the one of the prototypes presented in [18], [19], [39]. Those encoders exhibit a competitive DPS, but only one bit per row is accommodated in the encoders proposed in [18], [19], [39], contrary to the very competitive number (8.78 bits) achieved in this work. With the achieved bits per row, it is possible to assign a unique ID code to the different positions, and thus such encoder system can be considered to be absolute, contrary to previous systems (e.g., [23]), designated as quasi-absolute, as far as the ID codes of the different positions were inferred by reading a certain sequence of precedent $N-1$ bits (the whole encoder needs to be encoded with the so-called De Bruijn sequence, as detailed, e.g., in [23]).

Table 1 summarizes the performance and characteristics of various linear electromagnetic encoders (note that a quantitative comparison with other type of encoders based on different principles is meaningless). Some of the reported prototypes were considered for near-field chipless-RFID applications [36]-[39]. However, such encoders can be applied to motion control, and are therefore also included in the comparative Table 1. According to this table, the proposed encoder systems B' and B'' are very competitive, since both exhibit very high number of bits per encoder position (row) and an unprecedented DPL, the main FoM in electromagnetic encoders. The spatial resolution of encoder system B' and B'' is 0.5 cm and 0.3 cm, respectively, i.e., identical to the chains' period. With such resolution and the (indicated) 440 different positions with assigned ID code, it follows that the dynamic range of the encoder system B' is 220 cm, and it is 132 cm for the encoder system B''. With such a maximum dynamic range, the encoder position is unequivocally determined with a single ID code, and therefore the encoder can be categorized as absolute. Higher dynamic ranges with such resolution and system are possible, but then the system can no longer be considered absolute, but quasi-absolute, since a certain ID code does not univocally identify a single position (and therefore, after a system reset, the encoder should move various periods in order to determine their position).

With the previous dynamic ranges (220 cm for system B' and and 132 cm for system B'') and resolutions (0.5 cm and 0.3 cm for systems B' and B'', respectively), it follows that the proposed absolute encoders may find application as motion sensors in scenarios with moderate displacement spans and accuracy, encountered in many industrial systems. For very small displacements, other microwave sensors should be used, in particular, devices based on movable resonant elements (see, e.g., [40]-[45]).

B. Functionality as chipless-RFID system

As indicated before, some of the prototypes of Table 1 were designed for near-field chipless-RFID systems, rather than for measuring linear displacements and velocities. Indeed, the prototypes presented in this paper, as well as almost all the prototypes reported in Table 1, can also be considered for that purpose. Comparison of most reported electromagnetic encoders with other chipless-RFID systems, typically based on frequency domain [46]-[58], is meaningless, in general. However, since the proposed system uses also the frequency domain, plus the time domain, for encoding, it is interesting to compare the density per frequency (DPF) of frequency-domain chipless-RFID tags, with the DPF of any of the rows of the proposed system. In particular, for prototype B', such density is found to be DPF = 5.075 bit/GHz. In the reported frequency-domain chipless-RFID tags [46]-[58], there are systems that exhibit a superior DPF. For example, DPF = 25 bit/GHz in [48], a very competitive value. However, it should be emphasized that the DPF of prototype B' is for a single row, as mentioned. Such value (DPF = 5.075 bit/GHz) should be multiplied by the number of rows in order to obtain the real bit density per frequency of the encoder B'. Thus, the DPF can be made comparable, or even superior, to that of [48]. However, it should also be noted that, in the proposed system, the ID code of the whole tag (for a chipless-RFID application) is retrieved sequentially, row by row, through near field, different to the systems reported in [46]-[58].

Table 1. Comparison of various electromagnetic encoders.

Ref.	Sync.	Direction detection	Bits per row	DPS (bits/cm^2)	DPL (bits/cm)
[36]	Yes	No	1	0.60	0.67
[37]	Yes	No	1	1.15	1.67
[38]	Yes	No	1	1.19	1.72
[23]	Yes	Yes	1	0.76	2.29
[24]	Yes	Yes	1	1.63	6.96
[26]	Yes	Yes	1	0.8	2.42
[27]	Yes	Yes	1	0.8	2.4
[32]	Yes	No	2	0.89	2.5
[18]	No	No	1	7.45	16.7
[19]	No	No	1	26.0	16.7
[39]	No	No	1	4.90	16.7
[33]	Yes	No	2	1.67	5.0
[34]	Yes	No	2	3.34	10
[35]	Yes	No	4.58	0.70	4.58
A	**Yes**	**No**	**6.9**	**0.575**	**6.9**
B	**Yes**	**Yes**	**8.78**	**0.58**	**8.78**
B'	**Yes**	**Yes**	**8.78**	**1.17**	**17.56**
B''	**Yes**	**Yes**	**8.78**	**1.90**	**29.26**

VI. Conclusions

In conclusion, a strategy to significantly enhance the number of bits per row in electromagnetic encoders has been reported in this paper. The proposed system is based on four-chain encoders consisting of linear strips of different length. Such different lengths provide different notch frequencies when the strips lie on top of a transmission line and, thus, the frequency domain is used for encoding. The ID of the different rows (encoder positions), is retrieved sequentially, in a time-division multiplexing scheme similar to previous systems, but the number of bits per row is much higher by virtue of frequency encoding (through strip length) and thanks to the four chains per row considered. The system is intrinsically synchronous and does not need any additional chain for the generation of the clock signal, contrary to previous implementations. In the optimized prototype system, based on a reader consisting in a power splitter with four output ports, the achieved number of bits per row is 8.78 bits, and the data density per unit length, a figure of merit, is as high as DPL = 29.26 bit/cm in the optimized prototype, an unprecedented value in this type of encoders. With such number of bits per row, up to 440 different positions can be discerned. Thus, these encoders can be considered to be absolute, as far as the required number of positions to be identified by a unique ID code is inferior to that number.

References

[1] E. Eitel, "Basics of Rotary Encoders: Overview and New Technologies," *Machine Design Magazine*, vol. 4, no. 2, 2015.

[2] G. K. McMillan and D. M. Considine, "Process/Industrial Instrument and Control Handbook," in *Symposium A Quarterly Journal In Modern Foreign Literatures*, 1999.

[3] X. Li, J. Qi, Q. Zhang, and Y. Zhang, "Bias-tunable dual-mode ultraviolet photodetectors for photoelectric tachometer," *Appl. Phys. Lett.*, vol. 104, no. 4, paper 041108, 2014, doi: 10.1063/1.4863431.

[4] Z. Zhang, Y. Dong, F. Ni, M. Jin, and H. Liu, "A Method for Measurement of Absolute Angular Position and Application in a Novel Electromagnetic Encoder System," *J. Sensors*, vol. 2015, 2015, doi: 10.1155/2015/503852.

[5] Z. Zhang, F. Ni, Y. Dong, M. Jin, and H. Liu, "A novel absolute angular position sensor based on electromagnetism," *Sensors and Actuators, A: Physical*, vol. 194, 2013, doi: 10.1016/j.sna.2013.01.040.

[6] J. Jezný, and M. Curilla, "Position Measurement with Hall Effect Sensors", *Am. J. Mech. Eng*., vol. 1, pp. 231–235, 2013.

[7] P.N. Granell, G. Wang, G. S. Cañon Bermudez, T. Kosub, F. Golmar, L. Steren, J. Fassbender, and D. Makarov, "Highly compliant planar Hall effect sensor with sub 200 nT sensitivity," *Npj Flex. Electron*., vol. 3, p. 3, 2019.

[8] A. Lidozzi, L. Solero, F. Crescimbini, and A. Di Napoli, "SVM PMSM Drive with Low Resolution Hall-Effect Sensors," *IEEE Trans. Power Electr*., vol. 22, pp. 282–290, 2007.

[9] G. Scelba, G. De Donato, G. Scarcella, F. Giulii Capponi, and F. Bonaccorso, "Fault-Tolerant Rotor Position and Velocity Estimation Using Binary Hall-Effect Sensors for Low-Cost Vector Control Drives," *IEEE Trans. Ind. Appl*., vol. 50, pp. 3403–3413, 2014.

[10] X. Zhang, M. Mehrtash, M.B. Khamesee, "Dual-Axial Motion Control of a Magnetic Levitation System Using Hall-Effect Sensors," *IEEE/ASME Trans. Mechatron*., vol. 21, pp. 1129–1139, 2016.

[11] G. Liu, B. Chen, and X. Song, "High-Precision Speed and Position Estimation Based on Hall Vector Frequency Tracking for PMSM with Bipolar Hall-Effect Sensors," *IEEE Sens. J*., vol. 19, pp. 2347–2355, 2019.

[12] Rotary and Linear Motion Sensors. Available online: https://www.rls.si/eng/hilin (accessed on 17 January 2022).

[13] J. Naqui, F. Martín, "Application of broadside-coupled split ring resonator (BC-SRR) loaded transmission lines to the design of rotary encoders for space applications", *IEEE MTT-S Int. Microw. Symp*. (IMS'16), San Francisco, May 2016.

[14] J. Mata-Contreras, C. Herrojo, and F. Martín, "Application of split ring resonator (SRR) loaded transmission lines to the design of angular displacement and velocity sensors for space applications", *IEEE Trans. Microw. Theory Techn*., vol. 65, no. 11, pp. 4450-4460, Nov. 2017.

[15] C. Herrojo, J. Mata-Contreras, F. Paredes, F. Martín, "Microwave encoders for chipless RFID and angular velocity sensors based on S-shaped split ring resonators (S-SRRs)", *IEEE Sensors J*., vol. 17, pp. 4805-4813, Aug. 2017.

[16] J. Mata-Contreras, C. Herrojo, and F. Martín, "Detecting the rotation direction in contactless angular velocity sensors implemented with rotors loaded with multiple chains of split ring resonators (SRRs)", *IEEE Sensors J*., vol.18, no. 17, pp. 7055-7065, Sep. 2018.

[17] J. Mata-Contreras, C. Herrojo, F. Martín, "Electromagnetic rotary encoders based on split ring resonators (SRR) loaded microstrip lines", *IEEE MTT-S Int. Microw. Symp.* (IMS'18), Philadelphia, Pennsylvania, Jun. 2018.

[18] C. Herrojo, F. Muela, J. Mata-Contreras, F. Paredes, F. Martín, "High-density microwave encoders for motion control and near-field chipless-RFID", *IEEE Sensors J.*, vol. 19, pp. 3673-3682, May 2019.

[19] C. Herrojo, F. Paredes, and F. Martín, "Double-stub loaded microstrip line reader for very high data density microwave encoders", *IEEE Trans. Microw. Theory Techn.*, vol. 67, no. 9, pp. 3527-3536, Sep. 2019.

[20] C. Herrojo, F. Paredes, J. Mata-Contreras, F. Martín, "All-dielectric electromagnetic encoders based on permittivity contrast for displacement/velocity sensors and chipless-RFID tags*", IEEE-MTT-S Int. Microw. Symp.* (IMS'19), Boston (MA), USA, Jun. 2019.

[21] C. Herrojo, F. Paredes, and F. Martín, "3D-printed high data-density electromagnetic encoders based on permittivity contrast for motion control and chipless-RFID", *IEEE Trans. Microw. Theory Techn*., vol. 68, no. 5, pp. 1839-1850, May 2020.

[22] C. Herrojo, F. Paredes, and F. Martín "3D-printed all-dielectric electromagnetic encoders with synchronous reading for measuring displacements and velocities", *Sensors*, vol. 20, p. 4837, 2020.

[23] F. Paredes, C. Herrojo, F. Martín, "Microwave Encoders with Synchronous Reading and Direction Detection for Motion Control Applications", *2020 IEEE-MTT-S Int. Microw. Symp.* (IMS'20), Los Angeles, CA, USA, 21-26 Jun. 2020.

[24] C. Herrojo, F. Paredes, and F. Martín "Synchronism and Direction Detection in High-Resolution/High-Density Electromagnetic Encoders", *IEEE Sensors J*., vol. 21, no. 3, pp. 2873-2882, Feb. 2021.

[25] F. Paredes, C. Herrojo, F. Martín, "Position sensors for industrial applications based on electromagnetic encoders", *Sensors*, vol. 21, pp. 2738 (28 pages), 2021.

[26] F. Paredes, C. Herrojo, F. Martín, "3D-printed quasi-absolute electromagnètic encoders for chipless-RFID and motion control applications", *Electronics*, vol. 10, paper 1154, 2021.

[27] F. Paredes, C. Herrojo, A. Moya, M. Berenguel-Alonso, D. Gonzalez, J. Bruguera, C. Delgado-Simao, and F. Martín, "Electromagnetic Encoders Screen-Printed on Rubber Belts for Absolute Measurement of Position and Velocity", *Sensors*, vol. 22, paper 2044, 2022.

[28] F. Paredes, A. Karami-Horestani, and F. Martín, "Strategies to Enhance the Data Density in Synchronous Electromagnetic Encoders", *Sensors*, vol. 22, paper 4356, 2022.

[29] F. Martín, C. Herrojo, J. Mata-Contreras, F. Paredes, *Time-Domain Signature Barcodes for Chipless-RFID and Sensing Applications*, Springer, 2020.

[30] F. Martín, P. Vélez, J. Muñoz-Enano, L. Su, *Planar Microwave Sensors*, Wiley/IEEE Press, Hoboken, NJ, USA, 2022.

[31] N.C. de Bruijn, ""Acknowledgement of Priority to C. Flye Sainte-Marie on the counting of circular arrangements of 2n zeros and ones that show each n-letter word exactly once", *T.H.-Report 75-WSK-06*, Technological University Eindhoven, 1975.

[32] A. Karami-Horestani, F. Paredes and F. Martín, "A Hybrid Time/Frequency Domain Near-Field Chipless-RFID system", 21st Mediterranean Microwave Symposium, Pizzo Calabro, Italy, May 9-13, 2022.

[33] A. Karami-Horestani, F. Paredes and F. Martín, "Near-Field Hybrid (Time/Frequency Domain) Chipless-RFID System based on Linear Strips Tag", *10th Microwave & RADAR Week*, 12-14 Sep. 2022 Gdansk, Poland.

[34] A. Karami-Horestani, F. Paredes and F. Martín, "Frequency-coded and programmable synchronous electromagnètic encoders based on linear strips", *IEEE Sensors Lett*., vol. 6, no. 8, pp. 1-4, Art no. 3501704, Aug. 2022.

[35] A. Karami-Horestani, F. Paredes and F. Martín, "Near-Field Chipless-RFID System Based on Hybrid Time/Frequency Domain Encoding and Power Splitter Reader", *52nd Europ. Microw. Conf*., Milan, Italy, 20-25 Sep. 2022.

[36] F. Paredes, C. Herrojo, and F. Martin, "An approach for Synchronous Reading of Near-Field Chipless-RFID Tags", *10th IEEE International Conference on RFID Technology and Applications* (IEEE RFID-TA 2019), Pisa, Italy, 25-27 Sep. 2019.

[37] F. Paredes, C. Herrojo, and F. Martín, "High Data Density Near-Field Chipless-RFID Tags with Synchronous Reading", *IEEE J. RFID*, vol. 4, no. 4, pp. 517-524, Dec. 2020.

[38] F. Paredes, C. Herrojo, and F. Martín, "Microwave Encoders with Synchronous Reading and Direction Detection for Motion Control Applications", *URSI GASS 2020*, Rome, Italy, 29-5 Aug., 2020.

[39] J. Havlíček, C. Herrojo, F. Paredes, J. Mata-Contreras, F. Martín, "Enhancing the per-unit-length data density in near-field chipless-RFID systems with sequential bit reading", *IEEE Ant. Wireless Propag. Lett.*, vol. 18, pp. 89-92, Jan. 2019.

[40] J. Naqui, M. Durán-Sindreu, and F. Martín, "Alignment and position sensors based on split ring resonators," *Sensors*, vol. 12, pp. 11790–11797, 2012.

[41] A. Karami-Horestani, C. Fumeaux, S.F. Al-Sarawi, and D. Abbott, "Displacement sensor based on diamond-shaped tapered split ring resonator," *IEEE Sens. J*., vol. 13, pp. 1153–1160, 2013.

[42] A.K. Horestani, J. Naqui, D. Abbott, C. Fumeaux, and F. Martín, "Two-dimensional displacement and alignment sensor based on reflection coefficients of open microstrip lines loaded with split ring resonators," *Electron Lett*., vol. 50, pp. 620–622, 2014.

[43] A.K. Horestani, D. Abbott, and C. Fumeaux, "Rotation sensor based on horn-shaped split ring resonator," *IEEE Sens. J*., vol. 13, pp. 3014–3015, 2013.

[44] M. Elgeziry, F. Costa, and S. Genovesi, "Wireless Monitoring of Displacement Using Spiral Resonators," *IEEE Sens. J*., vol. 21, pp. 17838–17845, 2021.

[45] C. Mandel, B. Kubina, M. Schüßler, and R. Jakoby, "Passive chipless wireless sensor for two-dimensional displacement measurement," *Proc. Europ. Microw. Conf*., Manchester, UK, 10–13 Oct. 2011.

[46] I. Jalaly and I. D. Robertson, "RF barcodes using multiple frequency bands," in *Proc. 2005 IEEE MTT-S Int. Microwave Symp. Dig*., Long Beach, CA, pp. 139–142.

[47] S. Preradovic, I. Balbin, N. C. Karmakar, and G. F. Swiegers, "Multiresonator-based chipless RFID system for low-cost item tracking," *IEEE Trans. Microw. Theory Techn*., vol. 57, no. 5, pp. 1411–1419, May 2009.

[48]] J. McVay, A. Hoorfar, and N. Engheta, "Space-filling curve RFID tags," *Proc. 2006 IEEE Radio Wireless Symp*., pp. 199–202.

[49] A. Vena, E. Perret, and S. Tedjini, "A fully printable chipless RFID tag with detuning correction technique," *IEEE Microw. Compon. Lett*., vol. 22, no. 4, pp. 209–211, Apr. 2012.

[50] A. Vena, E. Perret, and S. Tedjini, "Design of compact and autocompensated single-layer chipless RFID tag," *IEEE Trans. Microw. Theory Techn*., vol. 60, no. 9, pp. 2913–2924, Sep. 2012.

[51] A. Vena, E. Perret, and S. Tedjini, "High-capacity chipless RFID tag insensitive to the polarization," *IEEE Trans. Ant. Propag*., vol. 60, no. 10, pp. 4509–4515, Oct. 2012.

[52] M. M. Khan, F. A. Tahir, M. F. Farooqui, A. Shamim, and H. M. Cheema, "3.56-bits/cm^2 compact inkjet printed and application specific chipless RFID tag," *IEEE Ant. Wireless Propag. Lett*., vol. 15, pp. 1109–1112, Oct. 2015.

[53] R. Rezaiesarlak and M. Manteghi, "Complex-natural-resonancebased design of chipless RFID tag for high-density data," *IEEE Trans. Ant. Propag*., vol. 62, no. 2, pp. 898–904, Feb. 2014.

[54] M. Svanda, J. Machac, M. Polivka, J. Havlicek., "A comparison of two ways to reducing the mutual coupling of chipless RFID tag scatterers," *Proc. 2016 21st Int. Conf. Microwave, Radar, and Wireless Communications* (MIKON), pp. 1–4.

[55] A. Vena, E. Perret, and S. Tedjini, "Chipless RFID tag using hybrid coding technique," *IEEE Trans. Microw. Theory Techn*., vol. 59, no. 12, pp. 3356–3364, Dec. 2011.

[56] M. A. Islam and N. C. Karmakar, "A novel compact printable dual-polarized chipless RFID system," *IEEE Trans. Microw. Theory Techn*., vol. 60, no. 7, pp. 2142–2151, July 2012.

[57] C. Herrojo, F. Paredes, J. Mata-Contreras, S. Zuffanelli, and F. Martín, "Multi-state multi-resonator spectral signature barcodes implemented by means of S-shaped split ring resonators (S-SRR)," *IEEE Trans. Microw. Theory Techn.*, vol. 65, no. 7, pp. 2341–2352, July 2017.

[58] O. Rance, R. Siragusa, P. Lemaître-Auger, and E. Perret, "Toward RCS magnitude level coding for chipless RFID*," IEEE Trans. Microw. Theory Techn*., vol. 64, no. 7, pp. 2315–2325, July 2016.

Amirhossein Karami Horestani has got his bachelor degree at 2015 in the field of biomedical engineering from the University of Isfahan. Then he studies at the university of Tehran in the field of micro/nano electronics for the master's degree until 2018. Since December 2021 he is working on microwave sensors and near field RFID systems as a PhD student at Universitat Autonoma de Barcelona.

Ferran Paredes (M'14-SM'22) received the Telecommunications Engineering degree from the Universitat Autònoma de Barcelona in 2006 and the PhD degree in Electronics Engineering from the same university in 2012. He is working as a Research Assistant at the Universitat Autònoma de Barcelona and his research interests include metamaterial concepts, passive microwaves devices, antennas, and RFID.

Ferran Martín (M'04-SM'08-F'12) was born in Barakaldo (Vizcaya), Spain in 1965. He received the B.S. Degree in Physics from the Universitat Autònoma de Barcelona (UAB) in 1988 and the PhD degree in 1992. From 1994 up to 2006 he was Associate Professor in Electronics at the Departament d'Enginyeria Electrònica (Universitat Autònoma de Barcelona), and since 2007 he is Full Professor of Electronics. In recent years, he has been involved in different research activities including modelling and simulation of electron devices for high frequency applications, millimeter wave and THz generation systems, and the application of electromagnetic bandgaps to microwave and millimeter wave circuits. He is now very active in the field of metamaterials and their application to the miniaturization and optimization of microwave circuits and antennas. Other topics of interest include microwave sensors and RFID systems, with special emphasis on the development of high data capacity chipless-RFID tags. He is the head of the Microwave Engineering, Metamaterials and Antennas Group (GEMMA Group) at UAB, and director of CIMITEC, a research Center on Metamaterials supported by TECNIO (Generalitat de Catalunya). He has organized several international events related to metamaterials and related topics, including Workshops at the IEEE International Microwave Symposium (years 2005 and 2007) and European Microwave Conference (2009, 2015 and 2017), and the Fifth International Congress on Advanced Electromagnetic Materials in Microwaves and Optics (Metamaterials 2011), where he acted as Chair of the Local Organizing Committee. He has acted as Guest Editor for six Special Issues on metamaterials and sensors in five International Journals. He has authored and co-authored over 650 technical conference, letter, journal papers and book chapters, he is co-author of the book on Metamaterials entitled *Metamaterials with Negative Parameters: Theory, Design and Microwave Applications* (John Wiley & Sons Inc.), author of the book *Artificial Transmission Lines for RF and Microwave Applications* (John Wiley & Sons Inc.), co-editor of the book *Balanced Microwave Filters* (Wiley/IEEE Press), co-author of the book *Time-Domain Signature Barcodes for Chipless-RFID and Sensing Applications* (Springer), and co-author of the book *Planar Microwave Sensors* (Wiley/IEEE Press). Ferran Martín has generated 22 PhDs, has filed several patents on metamaterials and has headed several Development Contracts.

Prof. Martín is a member of the IEEE Microwave Theory and Techniques Society (IEEE MTT-S). He is reviewer of the IEEE Transactions on Microwave Theory and Techniques and IEEE Microwave and Wireless Components Letters, among many other journals, and he serves as member of the Editorial Board of IET Microwaves, Antennas and Propagation, International Journal of RF and Microwave Computer-Aided Engineering, and Sensors. He is also a member of the Technical Committees of the European Microwave Conference (EuMC) and International Congress on Advanced Electromagnetic Materials in Microwaves and Optics (Metamaterials). Among his distinctions, Ferran Martín has received the 2006 Duran Farell Prize for Technological Research, he holds the *Parc de Recerca UAB – Santander* Technology Transfer Chair, and he has been the recipient of three ICREA ACADEMIA Awards (calls 2008, 2013 and 2018). He is Fellow of the IEEE and Fellow of the IET.